Complete canthi removal reveals that forces from the amnioserosa alone are sufficient to drive dorsal closure in *Drosophila*

Adrienne R. Wells[a,*], Roger S. Zou[a,*], U. Serdar Tulu[a], Adam C. Sokolow[b], Janice M. Crawford[a], Glenn S. Edwards[b], and Daniel P. Kiehart[a]
[a]Department of Biology and [b]Department of Physics, Duke University, Durham, NC 27708

ABSTRACT ***Drosophila*'s dorsal closure provides an excellent model system with which to analyze biomechanical processes during morphogenesis. During native closure, the amnioserosa, flanked by two lateral epidermal sheets, forms an eye-shaped opening with canthi at each corner. The dynamics of amnioserosa cells and actomyosin purse strings in the leading edges of epidermal cells promote closure, whereas the bulk of the lateral epidermis opposes closure. Canthi maintain purse string curvature (necessary for their dorsalward forces), and zipping at the canthi shortens leading edges, ensuring a continuous epithelium at closure completion. We investigated the requirement for intact canthi during closure with laser dissection approaches. Dissection of one or both canthi resulted in tissue recoil and flattening of each purse string. After recoil and a temporary pause, closure resumed at approximately native rates until slowing near the completion of closure. Thus the amnioserosa alone can drive closure after dissection of one or both canthi, requiring neither substantial purse string curvature nor zipping during the bulk of closure. How the embryo coordinates multiple, large forces (each of which is orders of magnitude greater than the net force) during native closure and is also resilient to multiple perturbations are key extant questions.**

Monitoring Editor
Richard Fehon
University of Chicago

Received: Jul 7, 2014
Revised: Sep 11, 2014
Accepted: Sep 12, 2014

INTRODUCTION

The coordinated cell shape changes and tissue movements of morphogenesis create complex multicellular organisms. Tracking the geometry of specific cell shape changes and movements (kinematics) and experimental manipulation of the processes that specify and drive such movements collectively reveal the biomechanical forces (dynamics) for morphogenesis and the formation of complex tissue structures (Keller *et al.*, 2003; Gorfinkiel *et al.*, 2011; Lecuit *et al.*, 2011; Fischer *et al.*, 2014). The mechanisms that allow morphogenesis to be both robust and resilient in the face of both natural (e.g., environmental and genetic) and experimental challenges are not fully understood.

The dorsal closure stage of *Drosophila* embryogenesis provides an excellent model system for studying cell sheet morphogenesis (Kiehart *et al.*, 2000; Harden, 2002; Harris *et al.*, 2009; Belacortu and Paricio, 2011; Gorfinkiel *et al.*, 2011). Comparable morphogenic movements are conserved across phylogeny and include vertebrate cell sheet movements that lead to neural tube and palate formation (Copp and Greene, 2013; Seelan *et al.*, 2013; Martin and Goldstein, 2014; Razzell *et al.*, 2014). During dorsal closure, individual amnioserosa cells can be tracked with fluorescence time-lapse microscopy, and the process of closure is readily interrogated using a variety of experimental approaches (reviewed most recently in Gorfinkiel *et al.*, 2011). A number of key molecular players that are required for dorsal closure have been identified genetically (Narasimha *et al.*, 2004, 2008; Harris *et al.*, 2009; Belacortu and Paricio, 2011; Miller and Davidson, 2013), and the relative forces that are required for closure have been defined using biophysical approaches (see later discussion; Kiehart *et al.*, 2000; Hutson *et al.*, 2003; Peralta *et al.*, 2007; Toyama *et al.*, 2008; Solon *et al.*, 2009; Ma *et al.*, 2009; Sokolow *et al.*, 2012; Saravanan *et al.*, 2013). Recently, various quantitative models of closure that combine experimental perturbations

This article was published online ahead of print in MBoC in Press (http://www.molbiolcell.org/cgi/doi/10.1091/mbc.E14-07-1190) on September 24, 2014.

*These are co–first authors.

Address correspondence to: Daniel P. Kiehart (dkiehart@duke.edu).

Abbreviations used: ABD, actin-binding domain; AS, amnioserosa; CA, canthi; DE-cadherin, Drosophila E-cadherin; DFT, discrete Fourier transform; GFP, green fluorescent protein; H, height; LE, leading edge; SGMCA, sqh promoter–driven GFP-tagged actin-binding region of *Drosophila* moesin.

and analysis with mathematical modeling have begun to emerge (Hutson *et al.*, 2003; Peralta *et al.*, 2008; Gorfinkiel *et al.*, 2009; Layton *et al.*, 2009; Solon *et al.*, 2009; Ma *et al.*, 2009; Almeida *et al.*, 2011; Wang *et al.*, 2012; David *et al.*, 2013; Jayasinghe *et al.*, 2013; Saravanan *et al.*, 2013).

Two biomechanical processes contribute the vast majority of the forces that drive closure. They include the apical constrictions of amnioserosa cells (driven by junctional belts of actomyosin and transiently formed apical medial arrays of actomyosin) and contractility of the actomyosin-rich, supracellular purse strings (also known as actomyosin-rich cables) localized in the leading edges of the first row of lateral epidermal cells. A third biomechanical process is due to the bulk of the lateral epidermis, which contributes forces that impede closure. These lateral epidermal forces are almost certainly due to passive forces (e.g., forces due to viscosity and elastic and/or plastic deformations) and/or active forces (e.g., forces due to actomyosin) that resist stretching. The fourth biomechanical process is zipping, which ensures a seamless dorsal epithelium. In non–laser perturbed closure (which we define as "native" closure), zipping also contributes to closure by maintaining the curvature of the supracellular purse strings (Hutson *et al.*, 2003; Peralta *et al.*, 2007). So-called "force ladders" quantitatively relate the ratio of the forces that each of the first three of these processes contribute to dorsal closure. We demonstrated that dorsal closure occurs at native or near-native rates when zipping has been compromised by laser perturbation to the amnioserosa near one or both canthi (Hutson *et al.*, 2003; Peralta *et al.*, 2007). All four of these processes are involved in native closure, although no one process is absolutely required for closure; thus closure can be powered by either the supracellular purse strings or the amnioserosa, but closure fails if both processes are inhibited (Kiehart *et al.*, 2000).

The dorsalward movement of a leading edge at the maximum dorsal opening is described by Newton's third law at low Reynolds number, i.e., $\sigma_{LE} - \sigma_{AS} - T\kappa = bv$ (Hutson *et al.*, 2003; Peralta *et al.*, 2007; Lu, Sokolow, Kiehart, and Edwards, unpublished data). These quantities are defined as follows: σ_{LE} is force per unit length acting on a leading edge of the lateral epidermis; σ_{AS} is the force per unit length provided by the amnioserosa; T is the tension in the purse string/actomyosin-rich cable; κ is the curvature of the cable (where $\kappa = 1/r$ and r is the radius of curvature of the arced purse string); $T\kappa$ is the force per unit length due to the purse string resolved in the direction of closure, that is, a direction normal to the anterior–posterior axis of the embryo; and b is the drag coefficient and v the velocity, such that bv is the drag acting on a unit length of the leading edge. It is important to note that each of the quantities σ_{LE}, σ_{AS}, and $T\kappa$ is two to three orders of magnitude larger than their sum (σ_{AS} and $T\kappa$ collaborate to drive closure, whereas σ_{LE} resists it). In addition, T is the largest force present, although only a fraction of this force is resolved in the direction of movement, such that the net force provided by the amnioserosa is approximately three times that provided by the purse strings (Hutson *et al.*, 2003; Peralta *et al.*, 2007). The force per unit length (stress) ladders quantify the ratios of the magnitudes of these quantities to within the following bounds (Hutson *et al.*, 2003; Peralta *et al.*, 2007):

$$\sim 510:380:130:1 \geq \sigma_{LE} : \sigma_{AS} : T\kappa : bv \geq \sim 490:380:130:1$$

The kinematics of zipping has been described both qualitatively and quantitatively (Jacinto *et al.*, 2000; Hutson *et al.*, 2003; Jankovics and Brunner, 2006; Peralta *et al.*, 2007, 2008; Toyama *et al.*, 2008; Almeida *et al.*, 2011). Zipping is impaired without myosin II function in the leading edge cells near the canthus region (Franke *et al.*, 2005). This observation implies that contractility in the purse strings is required for zipping (an alternative explanation is that the geometry of the leading edge cells that lack myosin II prevents them from being properly incorporated into the canthi). Measurements of groups of leading edge cells during closure revealed that net constriction of the purse strings occurs not in the bulk of the purse strings, but instead almost exclusively near either canthus as part of the zipping process (Peralta *et al.*, 2008). Nevertheless, the subcellular, actomyosin-rich elements of the purse string in individual cells can reversibly contract along the entire length of the purse strings (Kiehart *et al.*, 2000; Franke *et al.*, 2005). Together these observations suggest that the zipping process provides two important contributions: drawing the leading edges into the seams (with forces expected to be comparable to that provided by T, the tension in the purse string; Peralta *et al.*, 2008) and subsequently holding these epidermal cell sheets together.

As mentioned, the dorsalward progress of the leading edge of the lateral epidermis is unimpeded when zipping is compromised by targeting the amnioserosa near one or both canthi (Hutson *et al.*, 2003; Peralta *et al.*, 2007). We previously inhibited zipping with single and double canthus nicking protocols, which required repeated ablation of amnioserosa cells near one or both canthi intermittently throughout the course of closure. In the double canthus nicking experiments, as closure progressed, the curvatures of the contractile purse strings/actin cables were dramatically altered: instead of an eye-shaped morphology, the dorsal opening, outlined by the supracellular purse strings, acquired an hourglass-like geometry (e.g., Figure 1C in Hutson *et al.*, 2003, and Figure 5 in Peralta *et al.*, 2007). In this geometry, the apposing leading edge cells approached one another near the midpoint between the anterior and posterior ends of the dorsal opening. Ultimately the apposing leading edges met and commenced zipping. Of interest, this hourglass-like geometry resulted in purse string contractility that opposed, rather than favored, closure. In response to laser perturbation, the forces produced by the remaining amnioserosa were up-regulated such that the net result was that closure proceeded at nearly native rates (Hutson *et al.*, 2003; Peralta *et al.*, 2007). The mechanism by which the inhibition of zipping in double canthus nicking experiments results in amnioserosa force up-regulation is only partially understood. There is a correlation between force up-regulation and an increase in the rate of apoptosis in the amnioserosa (Peralta *et al.*, 2007; Toyama *et al.*, 2008), but the mechanism for regulating the rate of apoptosis remains unclear. Moreover, whether the increase in apoptosis can account for all of the up-regulation observed is also unclear.

Here we examine the combined roles of zipping and purse string curvature during dorsal closure with two novel laser protocols that dissect one or both canthi from the rest of the dorsal opening (Figures 1, A and B, and 2, A and B). The time course of the shape changes of the amnioserosa cells and the geometry of the leading edges were quantified. One key advantage for both protocols is the acute removal of one or both canthi, such that normal zipping and seam formation did not occur. A second key advantage is that the native curvature of the purse strings was not maintained after canthi removal. The purse strings recoil/shorten and flatten after the dissection of a canthus, reducing κ (and likely T), thus significantly reducing $T\kappa$, the dorsalward component of the force due to the purse string. Remarkably, even when segments of the apposing purse strings were parallel to each other (and the dorsal midline), progress of the leading edge toward the dorsal midline was maintained at native or nearly native (unperturbed) rates until the end stages of closure, when pronounced slowing occurred before the completion of closure. Thus closure can proceed in the absence of purse string curvature, which we

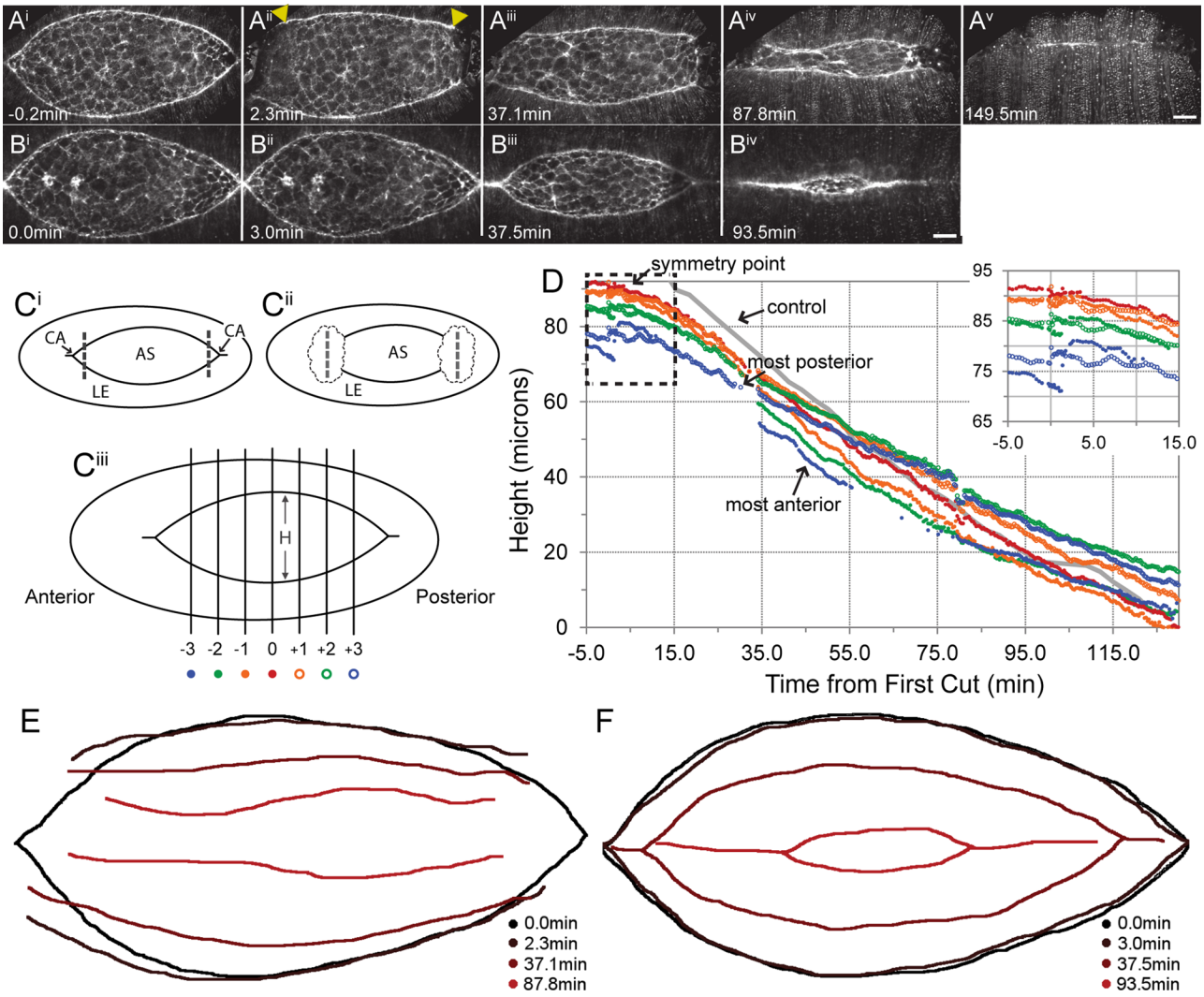

FIGURE 1: Canthus removal on an embryo early in closure results in flattening of the leading edges as they exhibit significant recoil, a temporary pause, and then near-native rates of closure. (A) Montage of time-lapse confocal micrographs of an embryo ubiquitously expressing GFP-moe-ABD to label F-actin (see Supplemental Movie S1 for its corresponding time-lapse video). Both canthi were removed by laser incisions. $t = 0$ marks the start of the first incision. Note the extensive ventralward recoil of leading edges near the incision sites for this embryo (yellow arrowheads) and the substantially flattened purse string minutes after incisions (between A^{i} and A^{ii}). (B) Montage of a native embryo expressing GFP-moe-ABD at similar time points as A (see Supplemental Movie S3 for its corresponding time-lapse video). (C) A canthus removal schematic represents a dorsal closure–staged embryo. Amnioserosa (AS), lateral epidermis (LE), canthi (CA), and the incisions (dashed lines) before (C^{i}) and after (C^{ii}) canthus removal. (C^{iii}) diagram of the dorsal opening illustrates the seven locations along the leading edges where height, *H*, was measured. (D) Plot of height vs. time for the embryo in A at positions diagrammed in C^{iii}. The gray height curve represents the native embryo in B. Inset (dashed box) of the time interval right before, during, and after canthus removal focuses on the sudden height increase caused by leading edge recoil (see jump on the plot represented by blue, closed circles). (E) Traces of the leading edges with different color for each time point in the montage during closure of the embryo in A. This further highlights the extensive ventralward recoil of the leading edges after canthus removal. (F) Same display as E for the native embryo in B. Scale bars, 20 μm (A^{v}, B^{iv}).

attribute to an increase in the force contribution from the amnioserosa. Quantitative analysis of amnioserosa cell shape shows changes in the length-to-width ratio of cells in approximately half of the dorsal opening closest to the removed canthus. In contrast, analysis of amnioserosa cell oscillations showed little or no change after canthus removal. Together our experiments confirm the robust nature of the dorsal closure process and support the existence of emergent properties that respond to alterations in purse string/actomyosin cable geometry to ensure successful closure.

RESULTS

Overview: after complete canthi removal, embryos recover and finish closure

To evaluate canthus function, we completely removed both canthi using laser dissection monitored by confocal time-lapsed microscopy ($n > 40$; Figures 1 and 2). The two canthi were removed sequentially during an interval of ~3–5 min. Each surgical incision was oriented perpendicular to the dorsal midline and spanned ~50 μm. The cuts were positioned ~10–12 μm inside of the targeted canthus,

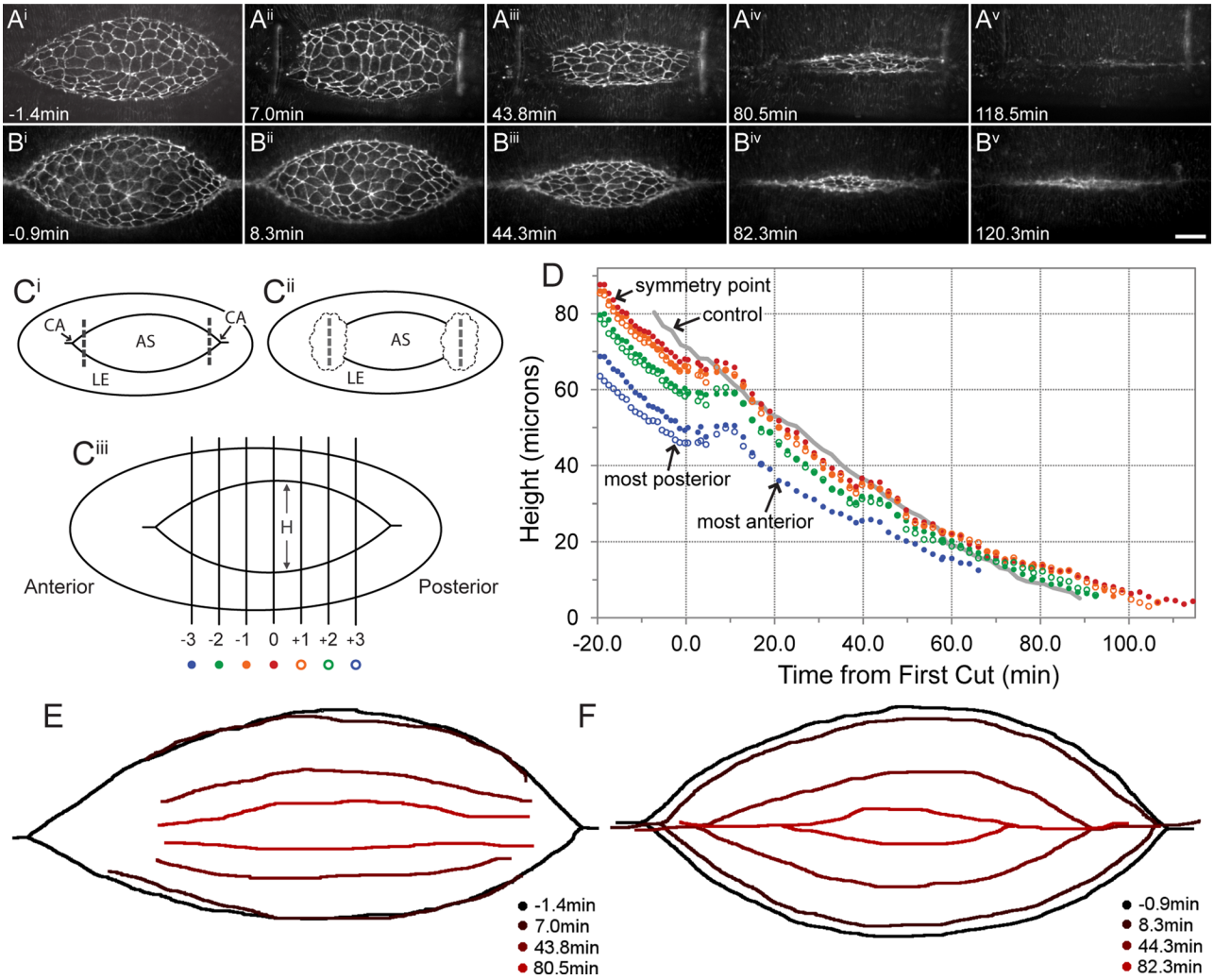

FIGURE 2: Canthus removal on an embryo in midclosure results in gradual flattening of leading edges, no significant ventralward recoil, and near-native rates of closure after short lag phase. (A) Time-lapse confocal micrograph montage of an embryo ubiquitously expressing *D*E-cadherin-GFP. Both canthi were removed by laser incisions. $t = 0$ signifies the start of the first incision. Note the minimal ventralward recoil of leading edges near the incision sites for this embryo (between A^{i} and A^{ii}; see Supplemental Movie S2 for its corresponding time-lapse video). (B) Montage of a native embryo expressing *D*E-cadherin-GFP at approximately the same time points as A (see Supplemental Movie S4 for its corresponding time-lapse video). (C) A canthus removal schematic representing a dorsal closure–staged embryo shown for reference (same as the schematic described in detail in Figure 1C). (D) Plot of height vs. time for the embryo in A at positions diagrammed in C^{iii}. The gray height curve represents the native embryo in B. (E) Traces of the leading edges with different color for each time point in the montage during closure of the embryo in A. This further highlights the lack of significant ventralward recoil of the leading edges after canthus removal. (F) Same display as E for the native embryo in B. Scale bar, 20 µm (B^{v}).

toward the center of the embryo (Figures 1C and 2C show schematics of cuts). The result of each laser incision was to cut a short dorsal region in the two lateral epidermal sheets, sever the supracellular purse strings at the leading edges of the two lateral epidermal cell sheets, and cut through the amnioserosa (Supplemental Movies S1 and S2). To ensure that the tissue was severed, the laser cut was sometimes repeated once or twice immediately after the first cut. Consequently, this laser surgery protocol reliably dissected the canthi from the bulk of the amnioserosa and both purse strings. It left an ablated region approximately ~20 µm wide after recoil, thereby ensuring complete physical and functional removal of the targeted canthus. Canthi removed from the remainder of the dorsal opening disappeared over the course of ~20 min. After the removal of both canthi, the leading edges recoiled away from the dorsal midline and shortened/recoiled along their contour length. They then stalled for ~5–10 min (see *Discussion*), after which time dorsal closure resumed and proceeded at nearly native rates until the end stages of closure (Figures 1D and 2D). At 20 min after the canthi were removed, the rate at which the height of the dorsal opening changes, dH/dt, for double canthus cut embryos was 18.2 ± 2.2 nm/s, compared with 19.2 ± 4.4 nm/s for controls. At 60 min, dH/dt for double canthus removed embryos was 8.0 ± 1.0 nm/s, whereas for controls it was 13.8 ± 0.3 nm/s (dH/dt for cadherin green fluorescent protein [GFP]–labeled embryos is typically faster than for GFP-moe ABD–labeled embryos, which we published previously; Hutson *et al.*, 2003). Note that in contrast to laser dissection of the purse string, which results

in the formation of a secondary purse string (Kiehart *et al.*, 2000, Rodriguez-Diaz *et al.*, 2008), we see little or no evidence for secondary purse string formation (i.e., tissue healing) upon dissection of the canthus.

It is of interest to note that the immediate response to canthus removal depends on the developmental stage of closure when the laser dissection was performed (compare Figures 1A and 2A and 1E and 2E; details are provided in the next section; see Supplemental Movies S1 and S2). In all embryos, the response to double canthus removal was greatest adjacent to the sites of the cuts and was minimal at the symmetry point (i.e., far from the site of the incision, near the center of the embryo; Figures 1E and 2E). In embryos cut early in closure, the purse strings began to flatten as they recoiled away from the dorsal midline (Figure 1D, inset). In contrast, when canthi were removed midway or later in closure, there was relatively little, if any, recoil (Figure 2D). After cuts in both early and mid dorsal closure–stage embryos, the purse strings continued to flatten with time as the process of closure proceeded (Figures 1A and 2A and 1E and 2E; detailed in the next section). In both early and mid dorsal closure–stage embryos, the purse strings recoiled along their contour length and flattened, that is, T decreased and the radius of curvature, *r*, of the purse strings increased (equivalently, the curvature κ decreased). We conclude that $T\kappa$, the force per unit length produced by the purse strings in the direction of closure, is reduced. When a segment of a leading edge becomes parallel to the dorsal midline, the local value of κ and thus $T\kappa$ becomes zero.

Without canthi, closure in virtually all embryos proceeded to completion. However, at the end stages of closure, *dH*/*dt* decreased relative to native closure (Figures 1D and 2D). Moreover, edge-to-edge connections were formed at a variety of different locations between the opposing parallel leading edges of the advancing lateral epidermal cell sheets (Supplemental Movies S1 and S2). Such edge-to-edge closure is in contrast to the majority of native closure, where seams are formed solely at the canthi during zipping. Nevertheless, such edge-to-edge closure is consistent with the final stages of native closure and with closure in double canthus nicked embryos (Peralta *et al.*, 2007; Rodriguez-Diaz *et al.*, 2008; Layton *et al.*, 2009). Just as in native closure, a seam rich in F-actin formed upon the completion of closure and then disappeared as the epithelial sheet became continuous and seamless. After closure was complete, embryos that underwent canthus removal continued to develop, most hatching into roaming larvae (26 of 30 hatched from their vitelline envelopes). The overall response to the canthus removal protocols was indistinguishable regardless of the GFP-fusion protein used for imaging purposes (GFP-moe-ABD for imaging F-actin, Figure 1, A and B, or *D*E-cadherin-GFP for imaging adherens junctions, Figure 2, A and B).

Characteristic, reproducible responses to complete canthus/canthi removal depend on the stage of dorsal closure

Embryos were staged by the height, *H*, of the dorsal opening (the greatest distance, perpendicular to the midline, between the opposing lateral epidermis leading edges). Embryos with $H > \sim 90$ μm were designated early stage, and those with $H < \sim 70$ μm were designated mid stage. We observed that the rate of closure varies depending on the genotype of the embryo imaged. sGMCA embryos close at a rate of ~0.012 μm/s, compared to *D*E-cadherin embryos, which close at a rate of ~0.018 μm/s.

Cuts made during early closure. There were two key changes to both purse strings near the targeted canthus during early stages of closure (Figure 1, E and F). The contour length of the purse string relaxed/shortened, and each purse string recoiled away from the dorsal midline in ventralward recoil. During these changes, both purse strings flattened. After these immediate changes, the purse strings continued to lose curvature over the course of ~55–65 min.

Cuts made during mid closure. The immediate response to canthus removal is dramatically different in mid closure–stage embryos compared with that of early stage embryos—shortening of the purse strings occurs, but recoil of the freed ends away from the dorsal midline is essentially nonexistent after cuts made in mid closure. Compare the embryo cut early in closure (Figure 1, A and E) to one cut late in closure (Figure 2, A and E).

Quantitative analysis of purse string morphology after double canthus cuts

To evaluate more quantitatively the effects of double canthus removal experiments, we characterized the effects of double canthus removal in greater detail when laser perturbation was performed midway through closure (Figure 3). The embryos were more precisely staged to improve reproducibility (see *Materials and Methods* and *Discussion*). We evaluated six embryos that were labeled with *D*E-cadherin-GFP and administered the laser protocol when the distance between the symmetry points of the leading edges (i.e., at the maximum dorsal opening) was 68 ± 1 μm, which is in the middle stage of closure. In each embryo, we selected six additional locations for height measurements—three on either side of the symmetry point (diagrammed in Figures 1C and 2C)—and plotted their heights over time (Figure 3B). The reproducibility of staged embryos is highlighted in Figure 3B, where the responses of all six embryos at a given position are shown on the same plot.

The most significant change in purse string geometry after canthi removal in mid stage embryos was the shortening of the purse strings. In contrast, there was little recoil of the leading edges away from the dorsal midline or changes in its curvature (compare Figure 1, E and F, to Figures 2, E and F, and 3A). These observations provide insight into the stage dependence of the mechanical properties of the tissues that affect dorsal closure (see also Rodriguez-Diaz *et al.*, 2008; Saravanan *et al.*, 2013).

Complete canthi removal causes purse strings to contract away from the incision site along their length

We measured the extent to which the leading edge contracts after canthus removal by following the movements of fiducials on or near the purse strings before, during, and after laser dissection. Four sets of fiducials were followed (each embryo has two purse strings, and the double canthus cuts free two ends on each purse string) on GFP-moe-ABD embryos. For each free end, three fiducials were tracked, and their distance to a fourth, reference fiducial was measured and plotted as a function of time (Figure 4, A–C). The reference fiducial was the one located farthest from the cut edge, closest to the symmetry point, and did not move much, if at all. The plots indicate that the purse strings rapidly shorten (arrows in Figure 4B confirming the observations in Figures 7 and 8 of Kiehart *et al.*, 2000). Moreover, the extent to which segments of the purse strings shorten is inversely proportional to the proximity of the segment to the cut end of the purse string (compare the movement of the fiducials and the extent of segment shortening in Figure 4B). These data are consistent with the embryo's response to other, noncanthi laser surgical cuts whereby there is little tissue movement >~50 μm from the cut. The shortening of the purse strings decreases the tension, T.

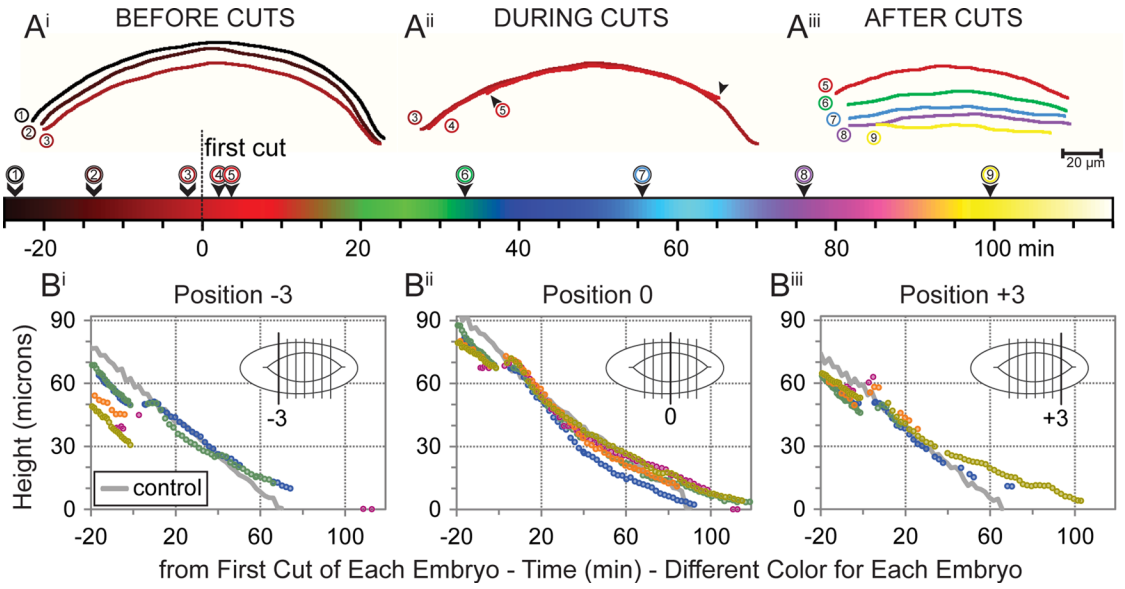

FIGURE 3: The leading edge response to canthus removal is most apparent near sites of incision. (A) Traces of one leading edge at different time points before, during, and after canthus removal. Traces are colored according to the time scale shown on the color bar. $t = 0$ marks the start of the first canthus cut. For reference, the last trace in A^{i} is repeated in A^{ii} with the same number, and the last trace in A^{ii} is repeated in A^{iii}. The right arrowhead in A^{ii} (posterior end) indicates part of leading edge that exhibits subtle ventralward recoil. Both arrowheads in A^{ii} exhibit retraction along the contour length of the leading edge. (B) Plots illustrate the similarity of responses that five individual embryos exhibit after the removal of both canthi. Each plot reports height measurements at a distinct location on five different embryos, each represented by a different color. The distinct location is illustrated in the inset of each plot, and all locations are illustrated in Figure $1C^{iii}$. Measurements from a native embryo are shown as a gray line in each plot.

These observations confirm that the leading edge is under tension and that during closure, individual cellular elements of the purse strings are stretched compared with their rest lengths (Kiehart *et al.*, 2000; Franke *et al.*, 2005; Rodriguez-Diaz *et al.*, 2008).

Purse strings flatten over time

Regardless of whether double canthus cuts were performed during early or mid stages of closure, the arced leading edges ultimately flattened. When cut early in closure, purse string flattening begins to occur immediately, during recoil from the microdissection. When cut in mid closure, virtually no flattening occurs during recoil (compare Figures 1E and 2E); nevertheless, the purse strings flattened after the net dorsalward movement of the leading edges resumed. We characterized the rate of flattening over the course of recoil and recovery by fitting the contours of the remaining leading edges to quadratic curves and then calculated the radius of a circular curve that best fit the quadratic approximation ($1/r = \kappa$; see fits in red overlaying the data in blue in Figure 4D). We found that it took approximately ~55–65 min for the leading edges to flatten (Figure 4, E and F).

Consequently, after double canthus cut experiments, the dorsalward forces supplied by the purse strings decrease substantially: because κ decreases and T likely decreases, so does their product $T\kappa$.

Canthus removal results in amnioserosa cell elongation in the ventralward direction and significant displacement away from the incision site

To ascertain more completely how early cuts affected the amnioserosa, we quantitatively evaluated both the overall shape of the amnioserosa and changes in the shape and position of individual amnioserosa cells by focusing on changes in the morphology of the dorsal opening after the removal of a single canthus (Supplemental Movie S5). The overall response of the dorsal opening to single canthus cuts was locally indistinguishable from that seen in double canthus cut embryos. The advantage of this approach is that cuts can be made more rapidly (within 1–2 min), and each embryo has both an experimental (i.e., cut) canthus and a control (i.e., native) canthus.

As described earlier, we used laser surgery to dissect a single canthus from the dorsal opening ($n = 8$; Figure 5, E and E′) and then investigated the consequences for the behavior of amnioserosa cells. We compared the amnioserosa cells in the last image taken before the cut (~30 s before) and the first image taken after the cut (~1–2 min after; Figure 5, E and E′). For native, uncut embryos, we chose images that differ over the same time interval as that of cut embryos (Figure 5, F and F′).

The most dramatic effect of the single-canthus cut was the displacement of centroids along the anterior–posterior axis away from the site of the cut (Figures 5, A and A′, and 6, A and A′). The centroids of cells closest to the dissected canthus were displaced the most. Moreover, the displacement of the centroids furthest from the cut (and nearest the intact canthus) appeared indistinguishable from that of unperturbed, native embryos. Indeed, we observed an inverse relationship between the displacement along the dorsal midline and the distance from the site of the cut that was well approximated by an exponential decay (Figure 6A; $n = 8$, $R^2 > 0.89$). This exponential decay was consistently observed for all embryos we examined, regardless of the stage of closure.

We also found that dissection of a canthus resulted in displacement of the centroids of the amnioserosa cells ventrally (perpendicular to the dorsal midline; Figures 5, B and B′, and 6, B and B′). In all the embryos we examined, there was more ventral displacement in cells close to the dissected canthus and near the purse strings

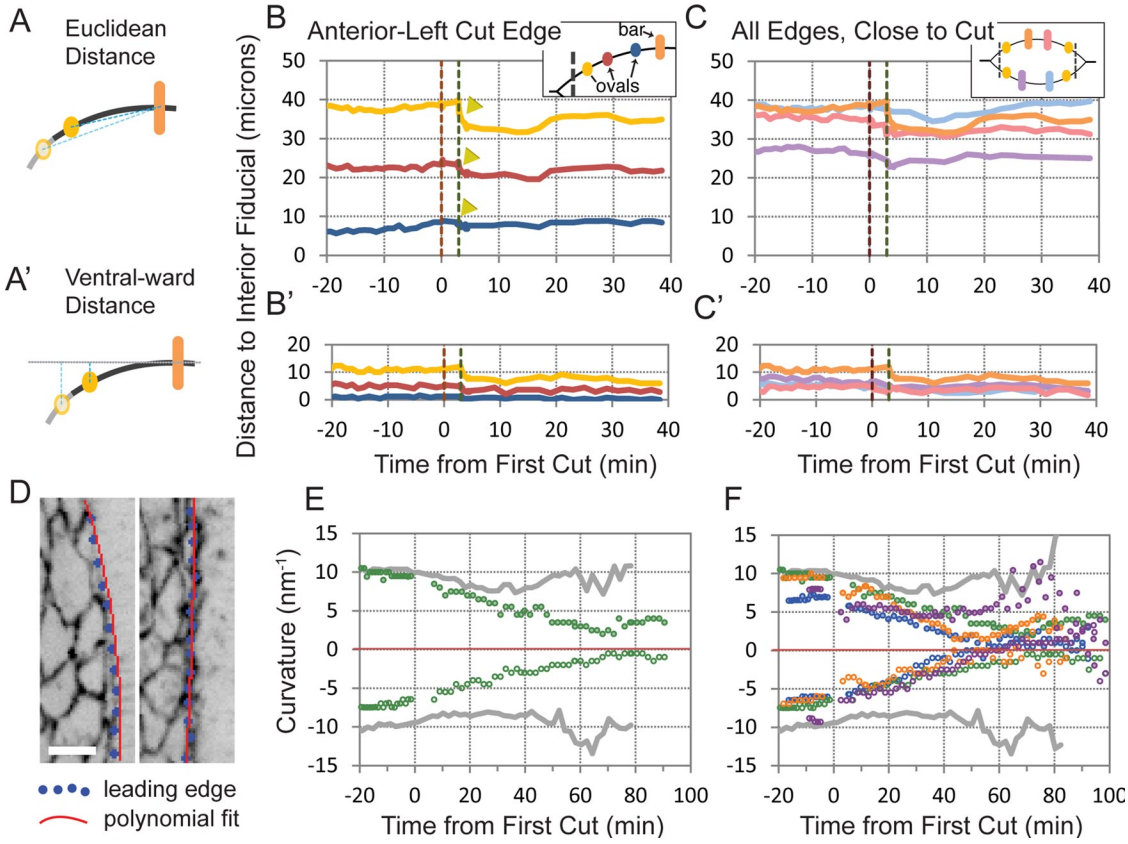

FIGURE 4: Leading edges recoil and flatten after canthus removal. Fiducials at cell–cell boundaries along each leading edge were tracked through time, including periods before, during, and after canthus removal procedures. (A, A′) Schematics illustrating Euclidean and ventralward distance measurements plotted over time (B, C and B′, C′, respectively. (B, B′) Plots report distance measurements between a reference fiducial (orange bar in inset) and three distinct fiducials (ovals in inset, in increasing distance from cut edge: yellow, red, blue) for the anterior-top, freed edge. Free edges refer to the leading edges detached from the canthus due to canthus removal. Yellow arrowheads show rapid shortening of purse strings. (C, C′) Plots compare distance measurements between each fiducial near freed edges (yellow ovals in inset) and its corresponding reference fiducial (bars in inset) in a single embryo. Colors in each plot correspond to distance measurements between the same-colored reference fiducial and the yellow fiducial proximal to the cut. The orange bar corresponds to the anterior-top free edge, pink to posterior-top, purple to anterior-bottom, and light blue to posterior-bottom. Vertical dashed lines in B, B′, C, and C′ indicate the start of the posterior (maroon) and anterior (green) canthus removal cuts. (D) Inverse images of a confocal fluorescence micrograph of an embryo ubiquitously expressing *D*E-cadherin-GFP before canthus removal (left) and after (right). Image overlay illustrates the procedure used to find leading edge curvature. A snakes (active contour) algorithm locates leading edges via optimally positioned snake points (blue dots). The snake points are fit to a polynomial (red lines), from which the curvature of the curve furthest from the midline is computed and plotted (E, F). (E) Plot of curvature over time for a double canthus removal embryo (green) and a native control embryo (gray). (F). Plot of curvature over time for four double canthus removal embryos (green, purple, orange, green) and control (gray). Scale bar, 10 μm (D).

(Figure 5B). Dissection of a canthus frees the two purse strings, which then shorten by recoiling along their contour length and in one way or another begin to flatten. Thus freeing the purse strings from the canthus releases tension, and shortening/flattening commences. The pulling force by a purse string propagates dorsalward through the amnioserosa, pulling hardest on amnioserosa cells neighboring a leading edge. These neighboring amnioserosa cells move with the recoiling leading edge and stretch in the L-R direction. Cells closer to the dorsal midline are pulled in both the L and the R direction by forces propagating from each purse string, respectively, and consequently stretch in the dorsal-ventral direction with minimal ventralward displacement. Stretching as a consequence of canthus dissection was evident within about half of the amnioserosa tissue (Figure 5, C and C′). In contrast, displacement of cells far from the cut site in laser surgically manipulated embryos appeared indistinguishable from the displacement of cells in unperturbed, native embryos (Figure 5, B and B′).

We further quantified the length-to-width ratio of each segmented amnioserosa cell in the images before and after canthus removal (Figure 6, C and C′). The ratio was determined by dividing the length of the cell measured along the dorsal-ventral axis (i.e., perpendicular to anterior posterior axis and the dorsal midline) by the length of the cell measured along the anterior-posterior axis (i.e., in the direction parallel to the dorsal midline). An increase in the length-to-width ratio indicates an increased component of ventralward stretching force that causes cell elongation. We consistently observed an increase in the length-to-width ratio for cells <50 μm from the site of the cut (Figures 5C and 6C) for all single canthus removal experiments. Within 50 μm from the cut site, the change in the length-to-width ratio was a function of the distance away from

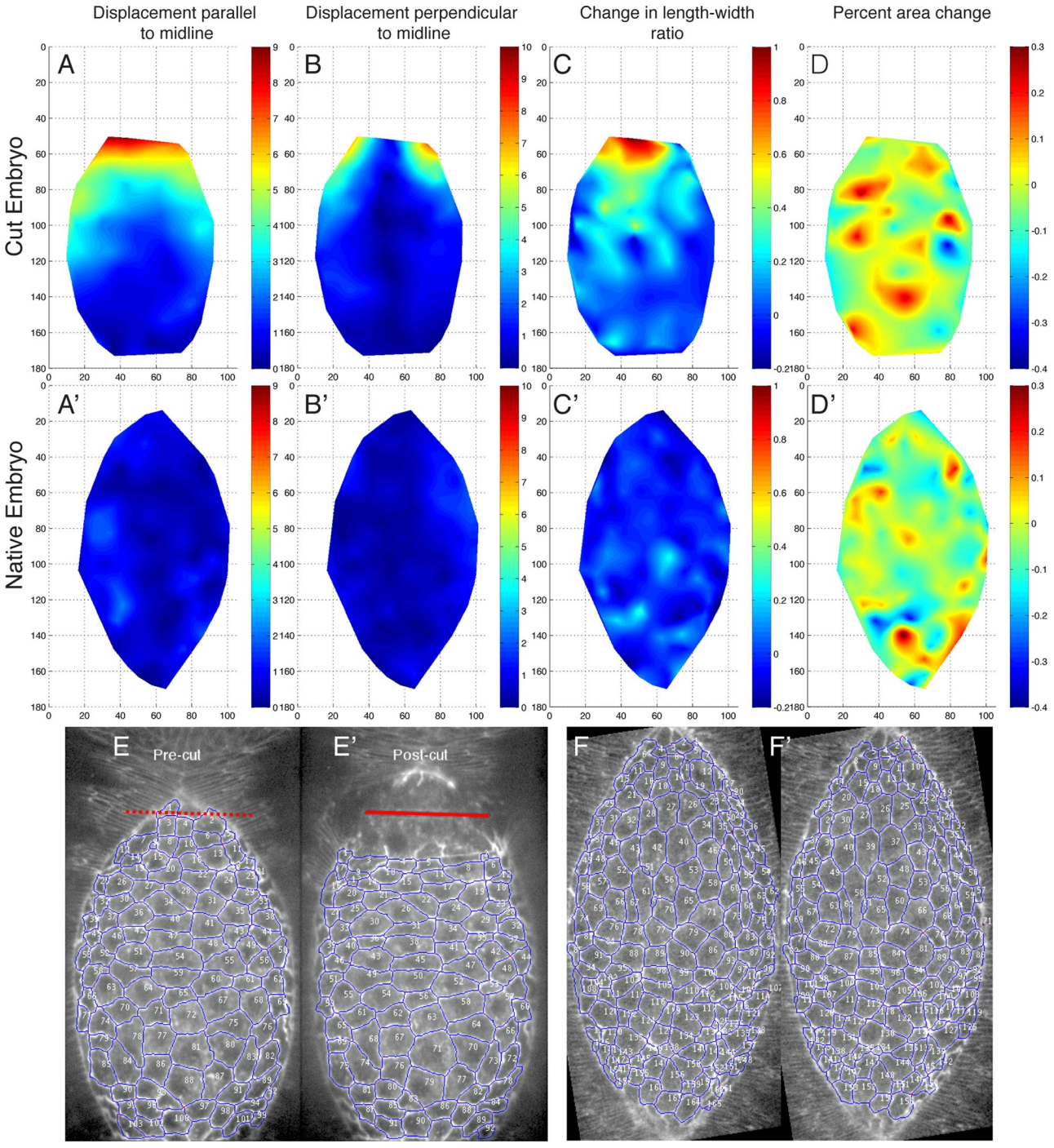

FIGURE 5: Removal of a single canthus causes amnioserosa cell recoil and ventralward tension. (A–D) Heat maps showing changes to different cell parameters in the amnioserosa cell sheet of an embryo before and after canthus removal and (A′–D′) in a native embryo over the same time interval. The "before" state was ~30 s before cutting, and the "after" state was ~1–2 min after the initial cut. (A) A heat map of amnioserosa cell centroid displacement (in micrometers) parallel to the dorsal midline (i.e., along anterior-posterior axis), both before and after canthus removal. (A′) Same measurement as A in a native embryo over the same time interval. (B) A heat map of amnioserosa cell centroid displacement (in micrometers) perpendicular to the dorsal midline (i.e., along dorsal-ventral axis), both before and after canthus removal. (B′) Same measurement as B in a native embryo over the same time interval. (C) A heat map of the change in amnioserosa cell length-to-width ratio before and after canthus removal. (C′) Same measurement as C in a native embryo over the same time interval. The length-to-width ratio is defined as the size of the cell in the dorsal-ventral axis over the size in the anterior-posterior axis. (D) Heat map of the percentage change in amnioserosa cell area before and after canthus removal. (D′) Same measurement as D in a native embryo over the same time interval. (E) Images of the embryo in A–D before canthus removal and (E′) after canthus removal. The red line denotes the site of laser incision. (F, F′) Images of the native embryo in A′–D′ over the same time interval as in E and E′.

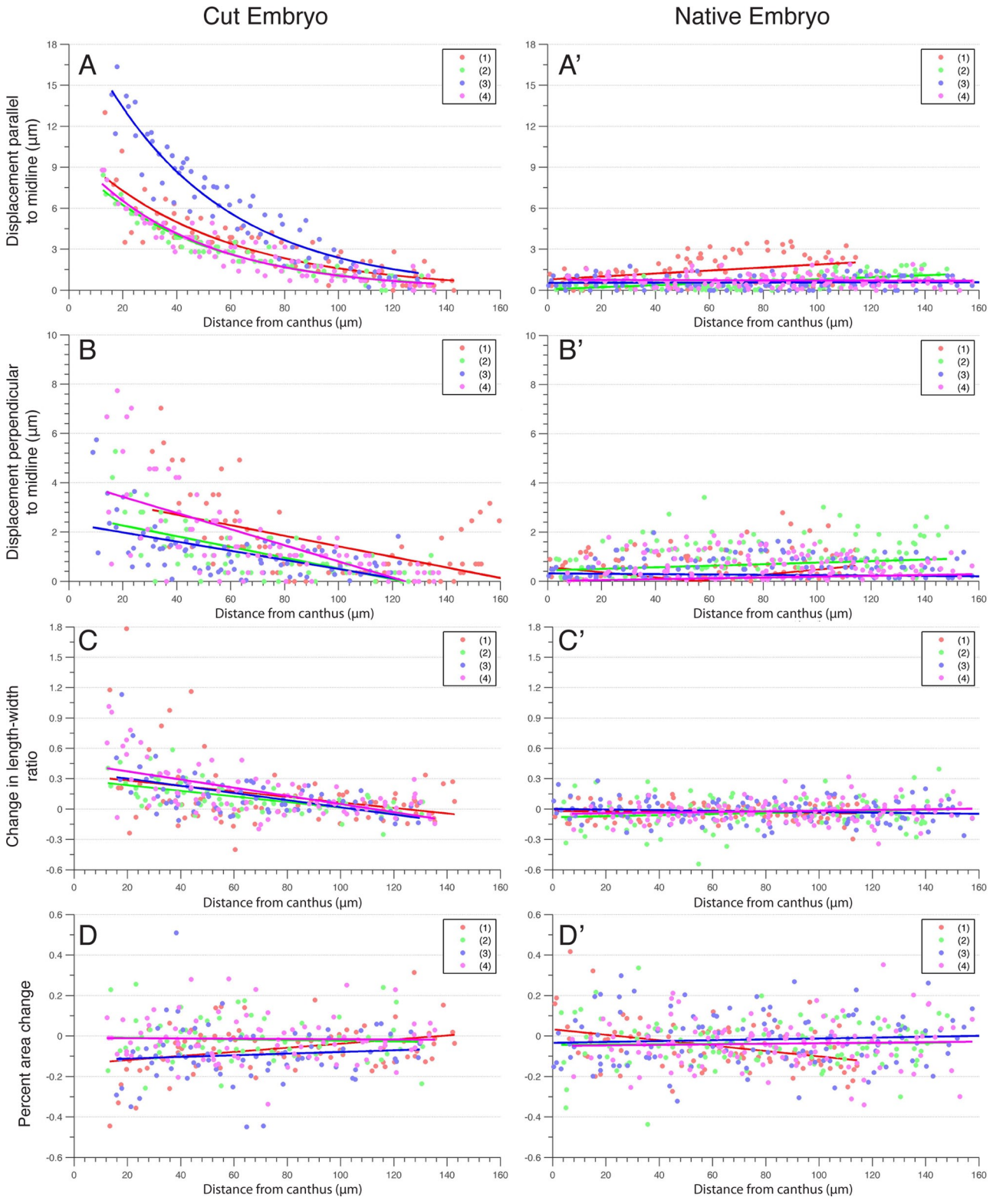

FIGURE 6: Effect of canthus removal on amnioserosa cell recoil and ventralward tension is a decreasing function of the initial distance away from incision site. (A–D) Plots of the amnioserosa cell parameters in the amnioserosa cell sheet before and after canthus removal as a function of distance from the site of incision in four single canthus–removal embryos and four native embryos (A′–D′) over the same time interval. The "before" state was ~30 s before cutting, and the "after" state was ~2–3 min after the initial cut. The "site of incision" reference point for native embryos is the relative position where a cut would occur. The plot of each embryo is labeled 1–4 with an assigned color. (A) Plot of the amnioserosa cell centroid displacement parallel to the dorsal midline (i.e., along anterior-posterior axis) both before and after canthus removal with respect to the initial distance from the cut site. (A′) Same measurement as A in a native embryo over the same time interval. (B) Plot of the amnioserosa cell centroid displacement (in micrometers) perpendicular to the midline (i.e., along dorsal-ventral axis) before and after canthus removal with respect to the initial

the cut site, with cells closest to the wound site exhibiting the most dramatic increase. The changes in the length-to-width ratios of cells >50 µm from the wound site were indistinguishable from the length-to-width ratios of cells in unperturbed control embryos (Figures 5C′ and 6C′). This indicates that the rebalancing of forces in the direction orthogonal to the dorsal midline due to the removal of one canthus subsequently causes amnioserosa cells to stretch along the dorsal-ventral axis.

Next we evaluated the change in amnioserosa cell area as a function of the proximity to the cut site (Figures 5, D and D′, and 6, D and D′). We quantified percentage area change between each cell before and after canthus removal and found that there was no observable difference for cells in canthus-removed versus native embryos. There was also no observable difference in the percentage area change for cells closer to and farther from the cut site. This behavior was consistent for all single canthus removal and uncut control embryos. Furthermore, a linear fit of the amnioserosa cell area change in each embryo revealed no appreciable difference in area change (Figure 6, D and D′). To evaluate the possibility of an increase in the variance of area change for cells closer to the wound, we categorized the cells by distance from the laser cut: 0– 4, 25–49, 50–99, and >100 µm. A Brown–Forsythe test for equality of group variances failed to indicate any significant differences between any of the category variances. Along with the length-to-width ratio observations discussed previously, this result indicates that amnioserosa cells close to the wound site are stretched perpendicular to the dorsal midline without a change in area. Assuming that the height (depth) of each amnioserosa cell is constant precut and postcut, this suggests that cell volume is preserved under single canthus removal by laser ablation conditions.

No change is observable in amnioserosa cell area oscillation amplitude or frequency due to canthus removal

We evaluated the oscillations in the apical cross section of the amnioserosa cells after canthus removal by tracking the change in area as a function of time with an automated cell segmentation program (see *Materials and Methods* and Supplemental Movie S6). The segmentation algorithm effectively tracked cell boundaries 30 min (after a 1– to 2-min delay) after laser dissection. Previous studies (Sokolow *et al.*, 2012) observed that individual amnioserosa cell oscillations in unperturbed embryos range from 4 to 10 mHz, which correspond to a 1.7- to 4.2-min period. Thus the 30-min window we specified can capture at least seven full cell oscillations. We observed no remarkable quantitative differences in frequencies or amplitudes of the area oscillations in amnioserosa cells adjacent to the site of laser dissection, far from that site, or in native embryos. This observation was consistent for all cut and native embryos (Figure 7).

To evaluate quantitatively the area time series, we used Fourier methods to measure oscillation frequencies. The time series of apical cross-sectional area exhibit low- and high-frequency bands that correspond to ingression and reversible oscillations, respectively (Sokolow *et al.*, 2012). The high-frequency band is due to the active forcing function along the perimeter of an amnioserosa cell. For each amnioserosa cell in each embryo, we estimated the high-frequency band and computed its discrete Fourier transform (DFT) during the first 30 min after dissection (Figure 8, D–D″). We compared the periodicity of amnioserosa cells in regions both near and away from the removed canthus, as well as the periodicity of cells in cut versus uncut embryos.

We found that the frequency distribution of the oscillations localized in the 4– to 10-mHz region for control embryos, which was consistent with results from Sokolow *et al.* (2012; Figure 8B′). Embryos with one canthus cut exhibited no distinguishable change in the frequency distribution compared with those of control embryos (also ~4–10 mHz; Figure 8C). The shape of the frequency distribution for each embryo increases rapidly at ~2 mHz and decays at higher frequencies (Figure 8, A, A′, B, and B′). The lack of signal in the low-frequency range (~0–3 mHz) is due to the polynomial curve fit that functions as a high-pass filter (Figure 8, D–D″). Our observations indicate that there is no observable change in the frequencies of reversible oscillations of apical cross-sectional area attributable to the canthus cut. However, these conclusions do not exclude the possibility that changes in the oscillation periodicity occur immediately after surgery but before we resume imaging (i.e., during the first 1–2 min after laser surgery).

We also explored the possibility that dissection of single and double canthi affected the rate of amnioserosa cell ingression. We determined the number and location of ingression events in each embryo over a 30-min interval and normalized the count by the total number of observed cells at the beginning of the interval (n = 10; unpublished data). We found no significant difference in the ingression rates between cut and native embryos, suggesting that the rate of apoptosis is not altered by these cuts. Furthermore, there appears to be no significant localization of ingression events to specific regions of the cut embryo (i.e., cells closer to the cut did not appear to ingress at a different rate).

In cut embryos that reestablish a balance of forces, amnioserosa cell centroids move comparably to centroids in uncut embryos

Finally, we investigated the position of the centroid of each tracked amnioserosa cell in cut embryos as a function of time after recoil and the observed pause in the dorsalward movement of the purse strings. Cells with the largest speeds were not localized to a specific region of the embryo or a specific window in time (Figure 9, A and A′, and Supplemental Movies S7 and S8). In Figure 9, cell trajectories are in false colors, with the color of this heat map indicating speed. We could not discern a pattern for the cells with the largest velocities in either laser-cut embryos or unperturbed native embryos. This suggests that after the initial recoil from canthus removal, external forces on the cell sheet rebalance, and each amnioserosa cell stabilizes by returning to native net movements over time.

DISCUSSION

Summary

We used two novel laser protocols to show that dorsal closure can recover the capability to progress at essentially native rates after the surgical removal of one or both canthi. These protocols acutely dissected the canthi from the key tissues that comprise the remainder

distance from the cut site. (B′) Same measurement as B in a native embryo over the same time interval. (C) Plot of change in the length-to-width ratio of the amnioserosa cells before and after canthus removal with respect to the initial distance from the cut site. (C′) Same measurement as C in a native embryo over the same time interval. (D) Plot of percentage change in the amnioserosa cell area before and after canthus removal with respect to the initial distance from the cut site. (D′) Same measurement as D in a native embryo over the same time interval.

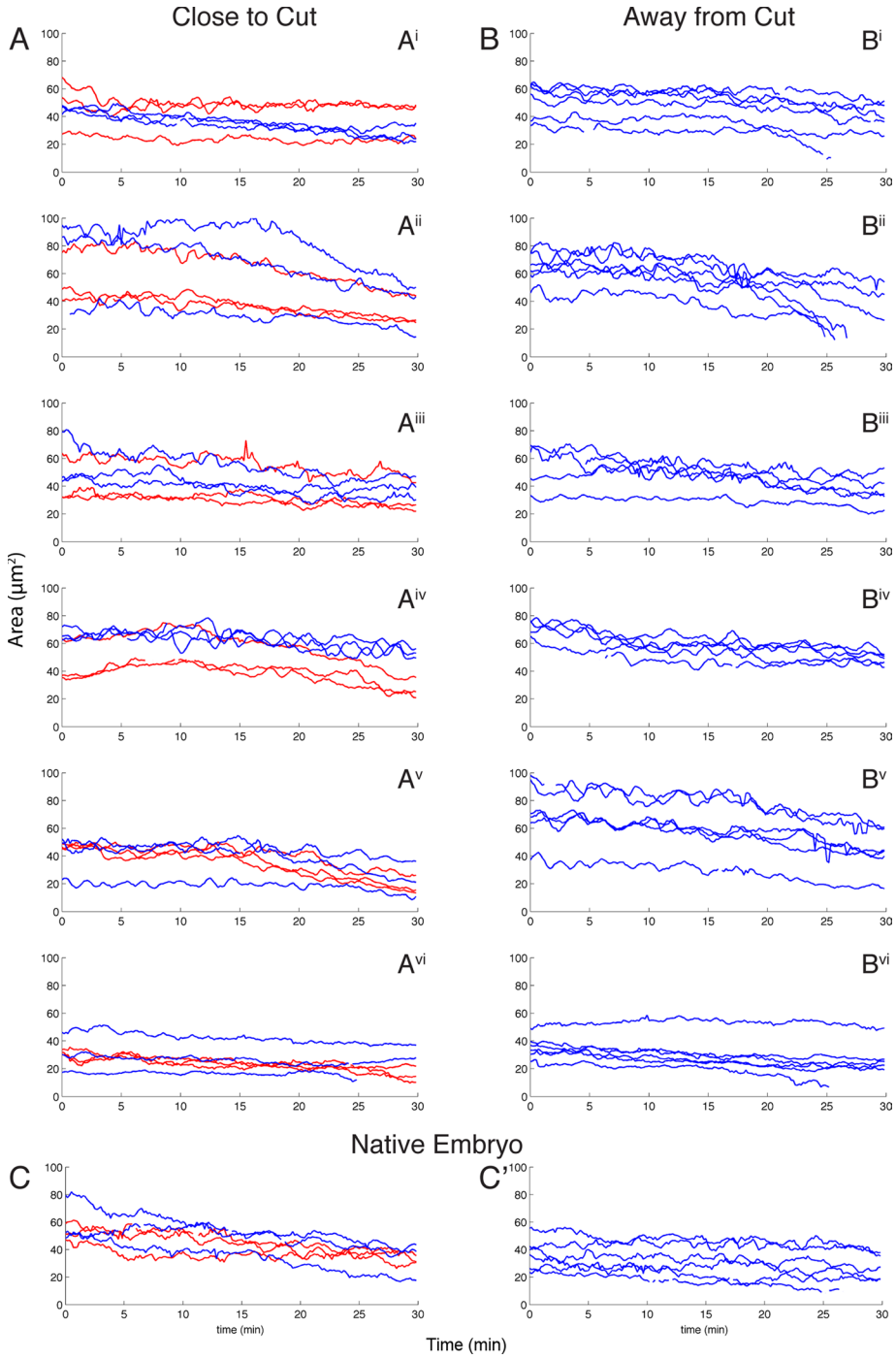

FIGURE 7: Area plots of amnioserosa cells indicate no noticeable short-term change in area oscillations as a result of canthus removal. (A, B) Graphs of amnioserosa cell area over time in six single canthus removal embryos. The time of the first image after canthus removal is $t = 0$. (A) Plot of the areas of three cells closest to the laser cut (red) and three cells slightly farther away from the laser cut (blue). (A^i–A^{vi}) Six different embryos. (B) Plot of cell area for the same six single cut embryos near the intact canthus (on the other side of the embryo). (C) Area plots of native embryos are qualitatively indistinguishable from the area plots in A and B. The "close to cut" and "away from cut" regions in native embryos refer to locations where a cut would have occurred had the embryo not been a control.

of the dorsal opening. Remarkably, after a brief delay that directly follows dissection, closure proceeds at native or nearly native rates until the end stages, when closure slows but nevertheless proceeds to completion. We conclude from these observations that, although the canthi are physically and functionally integrated into the tissues that are responsible for closure and contribute to native closure, they are not strictly required for the completion of perturbed closure.

When cuts are made early in closure, the dorsal opening rapidly relaxes to a new morphology as forces from the bulk of the lateral epidermis draw the purse strings ventrally. When cut during later stages of closure, relaxation to a new morphology occurs much more slowly (see later discussion). In either case, the geometry of the dorsal opening is dramatically different from that seen in native, wild-type embryos. In native embryos, the two purse strings converge at each canthus, and the two leading edges at the junctions of the amnioserosa and the lateral epidermis form the arcs of the eye-shaped dorsal opening. In contrast, in double canthus cut embryos, the arcs flatten with time so that the lateral epidermal cell sheets ultimately move toward the dorsal midline as more parallel fronts. As a consequence, the forces from the purse strings that contribute to closure in native, wild-type embryos are substantially reduced or eliminated. Thus, in the double canthus cut embryos, the amnioserosa alone must power closure until the end stages. The slowing of closure at end stages may occur before the formation of seams, during seam formation, and/or during their propagation through zipping (see also Peralta *et al.*, 2007; Rodriguez-Diaz *et al.*, 2008).

The amnioserosa cell sheet recoils away from the incision site and cells in nearly half of the amnioserosa tissue exhibit ventralward stretching. Once measurements were resumed (1–2 min after cuts), we observed no behavioral differences in the oscillations or rates of ingression of amnioserosa cells even though the morphology of the dorsal opening was dramatically altered. Moreover, amnioserosa cell movements appear essentially indistinguishable from their movement in native embryos.

New protocols and the dorsal-stage dependence of immediate recoil

Here we use novel laser protocols that completely dissect the canthi from the remainder of the tissues that contribute to dorsal closure. These protocols complement, contrast, and extend previous single and double canthus nicking protocols, which were designed to block zipping by perturbing the amnioserosa local to one or both canthi while preserving the canthi (Hutson *et al.*, 2003; Peralta *et al.*, 2007). In principle, these protocols could be used to interrogate closure from very early to very late stages (however, see experimental limitations for double canthus cuts performed on early embryos as detailed in *Materials and Methods*).

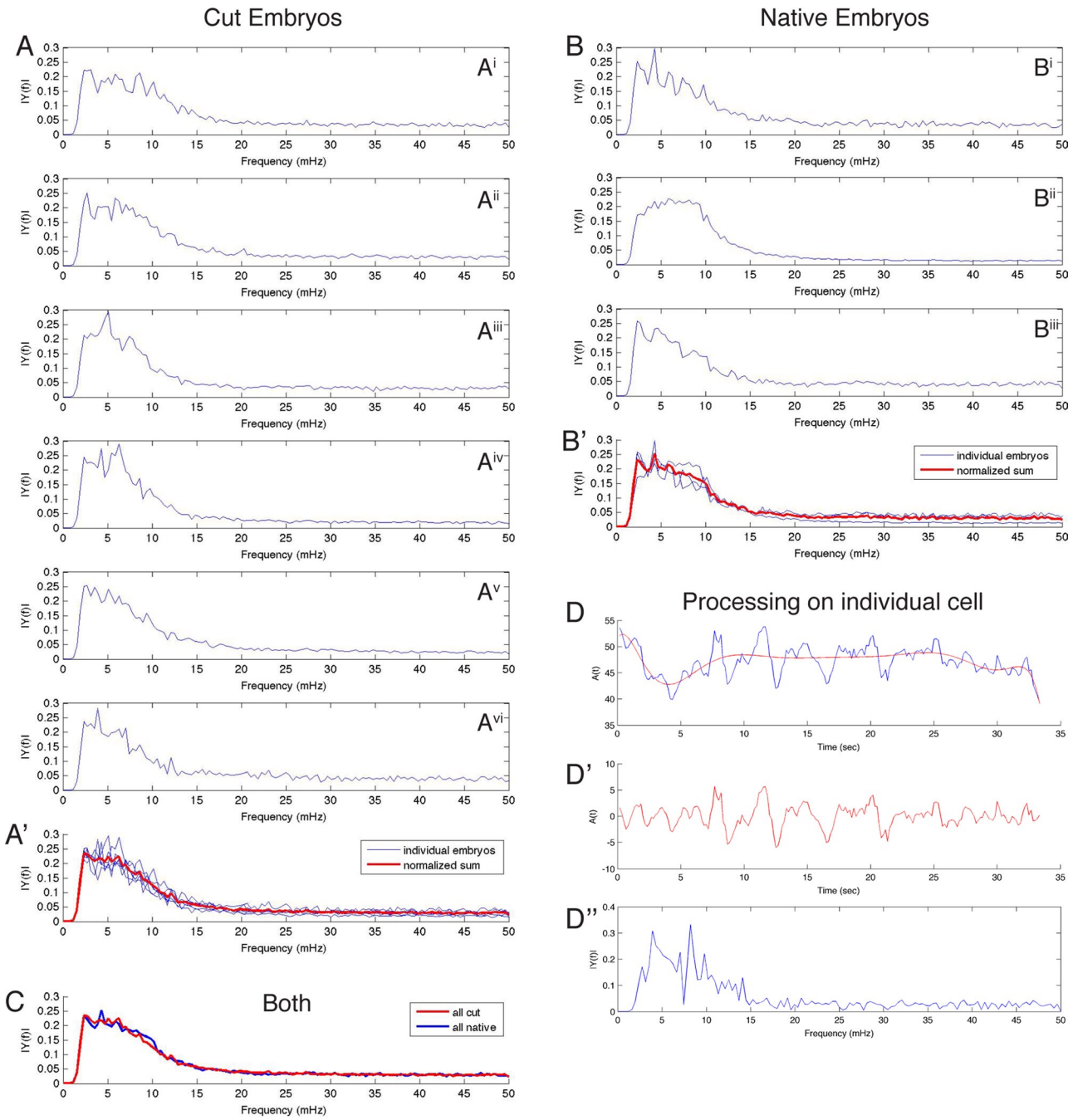

FIGURE 8: There is no observable effect on the cell area oscillation frequency after canthus removal. (A) Plots of cell areas of all tracked cells in the frequency domain for 30 min after canthus removal in each of six cut embryos (A^i–A^{vi}). (A′) Plot of cell areas in the frequency domain of all cut embryos is superimposed in blue, and the average of the blue curve is bold in red. (B, B′) Same measurements as in A and A′ for three native embryos (B^i–B^{iii}). (C) Plot of the normalized sum of area curves in the frequency domain between cut (red) and native (blue) embryos (red curve is bold red in A′, blue curve is bold red in B′). (D–D″) Steps in the area curve processing for Fourier analysis for an individual cell. (D) Blue curve is the original area curve in the spatial domain. The red curve is a polynomial fit of the area curve. (D′) Residual of area and polynomial fit in D. This procedure functions as a selective high-pass filter to enhance higher-frequency oscillations that represent the active oscillation in each cell. (D″) Fourier transform of D′. The process highlighted in D– D″ for each cell is used to generate plots of each embryo or of multiple embryos shown in A–C. That is, each plot in A′ and B′ includes all of the tracked cells in a given embryo.

The immediate response of the canthus removal experiments suggests that the epithelium itself becomes more rigid with time during development. More specifically, during early cuts, the purse strings recoil both away from the dorsal midline and along their contour length. In contrast, after cuts made later in closure, recoil is limited largely to shortening along the purse strings' contour length. These observations are consistent with a previous study that indicates a stage-dependent change in the material properties of the

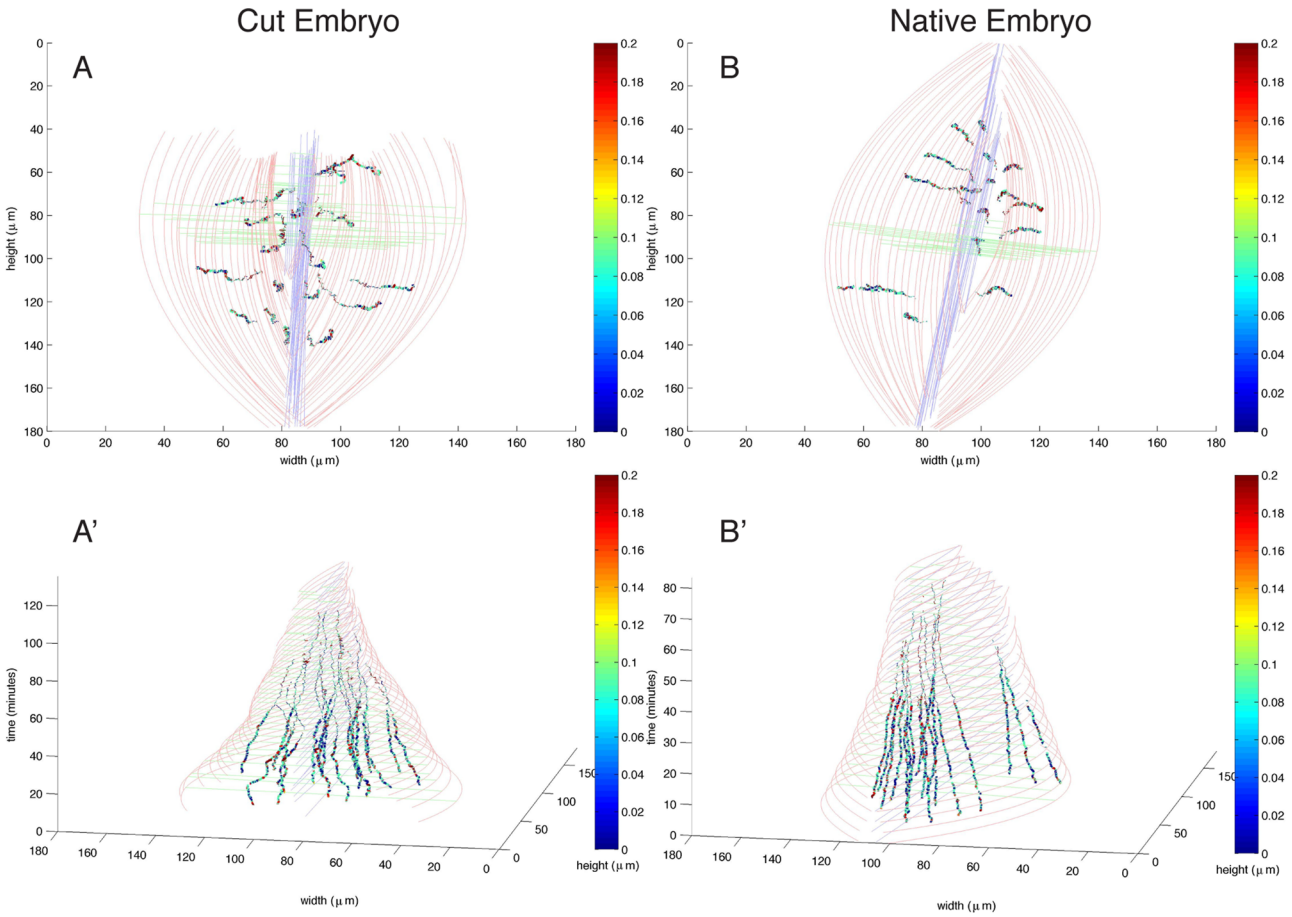

FIGURE 9: No noticeable change in centroid trajectories of amnioserosa cells follow canthus removal. (A, A′, B, B′) Three-dimensional (3D) representation of embryos with position in the *x*- and *y*-axes and time in the *z*-axis. (A, A′) The 3D representation of an embryo with one canthus removed, showing two different orientations. (A) Top view of A′ (see Supplemental Movie S7 for its corresponding video). (B, B′) The 3D representation of a native embryo showing the same two orientations as in A and A′ (see Supplemental Movie S8 for its corresponding video). The thin, grayish-red curves indicate the position of the leading edge over time as dorsal closure progresses. The thin blue lines trace the dorsal midline. The thin green lines orthogonal to the dorsal midline trace the length of greatest height (*H*) in the embryo. The dark traces with colors ranging from dark blue to red indicate the centroid velocities. "Warmer" false colors indicate faster velocities. The cells with faster velocities do not appear to be localized to any region in the space or time domain for both the cut and the uncut embryo. The velocity at each time point is computed as a moving average with a window size of 50 s. The cell centroid traces in the first 30 min are bold to indicate higher confidence in the accuracy of the trace. Cell tracking after 30 min deteriorates, and thus the cell centroid traces may not be as accurate (not bold).

amnioserosa (Ma *et al.*, 2009). Indeed, such stage dependence may reflect alterations in cytoskeletal function comparable to those observed by Fischer *et al.* (2014).

Pause before the resumption of closure

We do not fully understand why, after canthi removal, there is a 5- to 10-min pause after recoil and before the resumption of closure. We speculate that the rapid contraction of stretched arrays of actomyosin in the amnioserosa, the supracellular purse strings, and the lateral epidermis results in rearrangements in the contractile apparatus and a subsequent delay in the reengagement of closure. By this hypothesis, the pause represents a period during which contractile elements are reorganized so that they can participate effectively in the progress of closure under the constraints imposed by the new tissue geometry. Of interest, although the recoil, the pause, and the subsequent resumption of closure after canthus/canthi removal are consistent with tissue responses seen after microsurgery on the amnioserosa, the lateral epidermis, and/or the actomyosin purse strings (Kiehart *et al.*, 2000; Hutson *et al.*, 2003; Rodriguez-Diaz *et al.*, 2008), we do not see the formation of secondary purse strings associated with the single or double canthus cuts we describe here. When secondary purse strings do form after previously reported cuts to the lateral epidermis, they assemble within 2–5 min after laser cuts, and then after a delay of ~6 min, closure resumes (Rodriguez-Diaz *et al.*, 2008). Moreover, we see no other morphological indications of would healing but cannot rule out other wound healing events (e.g., the initiation of cell signaling cascades). This supports the notion that mechanisms other than secondary purse string formation drive dorsal closure in the absence of canthi.

Purse string curvature, zipping, and proposed ratchets

Formally, our experiments show that neither purse string curvature nor zipping is absolutely required for the bulk of cell sheet morphogenesis after laser dissection of both canthi. Previously we showed that the force produced by the amnioserosa can be up-regulated in

response to the double canthus nicking protocol (Peralta *et al.*, 2007; Toyama *et al.*, 2008), which may also be the case for the single or double canthus removal protocol. The slowing of closure we observe at the end stages suggests that zipping and/or purse string curvature may play an important role during the final stages of closure.

If the ratchet function that has been attributed to the purse strings (Solon *et al.*, 2009) requires global curvature of the purse strings, our observations provide evidence against such a ratchet function. Thus, our data would support the conclusions of other studies that call in question the role of the purse strings as ratchets for amnioserosa-based contractility (Gorfinkiel *et al.*, 2009, 2011; Spahn and Reuter, 2013). On the other hand, if ratchets require only local curvature, our data are consistent with their proposed mechanisms and would be consistent with the ratchet mechanisms documented previously (Solon *et al.*, 2009; Roh-Johnson *et al.*, 2012; Mason *et al.*, 2013). A more detailed analysis of local curvature after double canthus cut experiments performed at various times during closure might well be informative.

A new balance of forces follows canthus removal

Our analyses of closure after canthus removal reveals that closure can occur with little or no contribution from purse string contractility. We hypothesize that closure without canthi occurs due to up-regulating force in the amnioserosa, reducing opposing force from the lateral epidermis, or some combination of the two. Consistent with up-regulation of forces from the amnioserosa, we previously demonstrated that the force in the amnioserosa was up-regulated in response to the double canthus nicking protocol that also compromised purse string geometry (through inhibition of zipping; see prior discussion; Hutson *et al.*, 2003; Peralta *et al.*, 2007). To determine directly whether forces in the amnioserosa were up-regulated after canthus removal, we executed laser-effected mechanical jump strategies in an effort to measure recoil rates. Unfortunately, trauma due to surgery was too great. Embryos treated with this additional laser incision consistently blew out—they split open and leaked yolk contents, confounding instantaneous recoil measurements of amnioserosa tension release that are required to assess up-regulation of amnioserosal forces ($n = 4$). Moreover, our observation that recoil away from the dorsal midline does not occur after canthus removal during midclosure is unexpected. We do not understand how a new balance of forces drives closure at near-native rates and compensates for the lack of purse string curvature after canthus removal experiments.

Cell shape changes in the amnioserosa after single and double canthus removal experiments

Our results demonstrate that the most significant effect on the amnioserosa after complete canthus removal and leading edge flattening is the stretching of the amnioserosa cells. Cells in about half of the amnioserosa (closest to the incision site) in single canthus removal experiments were most strongly affected. Because we observe no increase in apoptotic ingression, we speculate that distorting amnioserosa cells through stretching may be an alternative mechanism for up-regulating force production. Indeed, such stretching may up-regulate amnioserosa force production through mechanically gated channels, recently implicated in closure (Hunter *et al.*, 2014). In contrast, we did not observe changes in cell oscillations (Fernandez *et al.*, 2007; David *et al.*, 2010; Blanchard *et al.*, 2010) or in the rate of ingression, the latter being correlated with the force produced by the amnioserosa (Toyama *et al.*, 2008). Therefore any change in force contribution by the amnioserosa and/or lateral epidermis that compensates for the altered purse string geometry after canthus removal must occur while maintaining native amnioserosa cell shape characteristics.

Emergent properties and a conceptual model for dorsal closure

Dorsal closure is a cell sheet movement with many properties that recapitulate those found in vertebrates during such morphogenic movements as neural tube closure and palate formation. Nonperturbed, native closure is a consequence of three active processes that promote closure. 1) In the amnioserosa, cellular forces provided by contractile actomyosin in the junctional belts and apical medial arrays sum to $\sigma_{AS}ds$. 2) In the purse strings, the actomyosin contractility at the leading edge of the lateral epidermis provides T (and therefore $T\kappa$). 3) Canthi provide structures that coordinate the overall geometry of the purse strings and zip together the two flanks of lateral epidermis into seams. Thus, during native closure, these three active processes, together with the force generated by of each flank of the lateral epidermis ($\sigma_{LE}ds$), constitute a biomechanical system.

In nonperturbed, native embryos, biophysical studies indicate that the purse strings contribute a substantial fraction of the forces required for native closure and that the individual forces that contribute to closure are two to three orders of magnitude larger than the net force that drives closure (Hutson *et al.*, 2003; Peralta *et al.*, 2007). During native closure, the canthi maintain the arc of each purse string, which leads to a component of purse string tension ($T\kappa$) throughout each leading edge that promotes closure. In addition, zipping forces contribute to the irreversible contraction of the width of a leading edge cell as it is incorporated into a seam as part of the zipping process (Peralta *et al.*, 2007). Forces from amnioserosa cells are provided by both apical medial arrays of actomyosin and junctional belts of actomyosin (Ma *et al.*, 2009; David *et al.*, 2010; Blanchard *et al.*, 2010) and provide the other major force contributing to closure.

Here we use double and single canthus cut protocols to demonstrate that neither zipping nor purse string curvature is absolutely required for dorsal closure and that dorsal closure resumes at rates indistinguishable from that for native embryos until the end stages of closure. We conclude that forces from the amnioserosa must be up-regulated but do not understand how. Previously we demonstrated that after laser removal of the amnioserosa, dorsal closure also progresses, albeit with delayed zipping rates (see Figure 4 and the discussion of Eq. 2 in Hutson *et al.*, 2003). Moreover, the slowing of closure at end stages in canthus cut embryos reveals forces associated with zipping that are otherwise small compared with the other forces involved. Finally, no single one of the four processes is either required or sufficient for the progress of dorsal closure. However, perturbation of multiple processes can compromise closure (Kiehart *et al.*, 2000; Hutson *et al.*, 2003). We infer that regulation of dorsal closure must require emergent properties that integrate appropriate cellular functions to make this morphogenetic process the redundant, robust, and resilient process that it is. The nature of such properties remains a key extant research question.

MATERIALS AND METHODS

Drosophila strains

All experiments were performed on two transgenic strains of *Drosophila* embryos. *D*E-cadherin-GFP expression is driven by a ubiquitin promoter/enhancer cassette (Oda and Tsukita, 1999, 2001) and labels cadherin-rich cell–cell junctions. The F-action label, *s*GMCA, is a fusion of the F-actin binding domain of *Drosophila*

moesin with GFP (Kiehart *et al.*, 2000) and is expressed under the control of the *spaghetti squash* (nonmuscle myosin II regulatory light chain) promoter/enhancer cassette (and is therefore essentially ubiquitously expressed). It is important to note that native embryos labeled with *s*GMCA close more slowly (~12 nm/s) than those labeled with *D*E-cadherin-GFP (~18 nm/s).

Embryo preparation

Flies were maintained using standard methods, and embryos were collected with small population cages on grape agar plates and yeast paste (Roberts, 1998). Embryos were prepared for laser surgery using methods described previously (Kiehart *et al.*, 2006). Dechorionated embryos were transferred to a grape-agar pad, and dorsal closure–stage embryos were selected and oriented dorsal side up in a line. A coverslip coated with "embryo glue" was used to pick up the line of embryos. The coverslip was placed, embryos down, on the gas-permeable Teflon membrane of a custom chamber containing a drop of a halocarbon oil mixture (1:1 HC100 and HC70; Kiehart *et al.*, 2006). A small amount of pressure was carefully applied to the coverslip to distribute the oil and slightly flatten the dorsal surface of the embryo onto the coverslip; this aided in imaging by making more of the dorsal opening visible in a minimum number of *z*-plane, optical sections. Gentle flattening is benign—virtually all embryos hatch and, if rescued from the halocarbon and placed in a food vial, develop into fertile adults.

Confocal microscopy and laser microsurgery

Confocal fluorescence imaging and laser microsurgery were performed as previously described (Kiehart *et al.*, 2006). Fluorescence images for all microsurgery experiments were acquired with a 40× water emersion, 1.2 numerical aperture objective on a Zeiss Axioplan or Axio Imager.M2m upright microscope equipped with a Yokogawa CS-10 spinning-disk confocal head. Laser microsurgery experiments used 355-nm light from a tripled Nd:YAG ablating beam (Minilite II, model YG571C; Continuum, San Jose, CA) as the ablating beam. This beam was expanded to match the rear aperture of the microscope objective and produced a near-diffraction-limited focal spot at the specimen plane.

Embryos were initially time-lapse imaged for 3–10 min at 1- to 2-min intervals to establish their unperturbed closure rate, stage, and native morphology. Imaging at 10- or 30-s intervals was used to capture amnioserosa cell behavior. Subsequent to presurgical imaging, the last image from the time-lapsed sequence was transferred to the computer controlling both the laser microbeam shutter and an actuated mirror that steers the microbeam across the specimen in a user-specified pattern. A line was drawn on the image perpendicular to the dorsal midline and ~30 pixels (12 ± 3 μm) inside the canthus (i.e., toward the middle of the embryo). This line, ~50 μm in length, was designed to sever the canthus away from the bulk of the dorsal opening. Once the pattern for the cut was established and the microbeam was set to fire, the imaging program was switched to image every 0.09 s, with image acquisition triggered by the pulses of the surgical laser (set to fire at 10 Hz), so that the camera shutter was closed when the surgical laser beam was on. Exposure times were reduced from ~250 to 70 ms. This allowed the embryo to be imaged while being cut; otherwise, 355-nm light–induced autofluorescence was strobed by the spinning disk and obscured images of the GFP fluorescence (we thank Rod Bunn of Vashaw Scientific, Norcross, GA, for helping us to arrange this method of eliminating this autofluorescent bloom). The array of lenses in the spinning disk that was strobed by the ultraviolet laser is shown in Supplemental Movie S1, taken before we implemented laser triggering of the camera shutter.

In double canthus cuts, the canthus was first removed from the posterior end of the dorsal opening. A new line was drawn on a freshly acquired image of the embryo, and a second cut was executed at the anterior side. Frequently, the focal plane had to be adjusted between the two separate incisions. To be certain that connections were severed between the canthi and the bulk of the amnioserosa and purse strings, surgical cuts were made one to three times on each side. Recoil away of the severed canthi from the bulk of the dorsal opening confirmed that mechanical attachments had been completely removed.

After both posterior and anterior cuts were completed, the imaging system was switched back to a longer exposure time and less frequent frame rate, and *z*-stacks were acquired until the completion of closure. Complete *z*-stacks were acquired at 1- to 2-min intervals to track leading-edge behavior and at 10- or 30-s intervals to track amnioserosa cell behavior. The next day, most slides were examined for hatch rates of imaged embryos. Of 30 embryos that underwent canthus removal, 26 hatched into roaming larvae. There were 40 double-canthus cuts and 20 single-canthus cuts in total.

In principle, double canthus cut experiments could be performed during all stages of dorsal closure. In practice, we find that early embryos are fragile and do not survive laser surgery as readily as do older embryos. We speculate that this is because 1) the overall geometry of the embryo and the dorsal opening are not readily amenable to canthus removal and 2) as dorsal closure proceeds, the epithelium becomes more robust. In early embryos, the dorsal opening is larger, and therefore the laser incision designed to sever the canthi from the remainder of the dorsal opening has to be longer. As a consequence, the cut extends to or near a region where the surface of the embryo curves up and away from the coverslip on which the dorsal surface is gently flattened. Observations of embryos that fail to survive the double or single canthus removal experiments suggest that failure occurs as a consequence of "blowout" by which cells and yolk flow out of the embryo at or near the site of the cut. Indeed, we find that blowout occurs most frequently when the cut approaches that part of the epithelium that no longer is tightly apposed to the coverslip. This occurs most frequently when cutting early closure–stage embryos.

In single-canthus cuts, the same procedure as double canthus cuts was repeated, except only one canthus on either the anterior or posterior end was removed. There were 20 single-canthus cuts in total.

dH/dt analysis of ubi-*D*E-cadherin-GFP embryos

The rate of dorsal closure in *s*GMCA embryos was measured by established methods; an active contours algorithm ("snakes") was applied to a time-lapse sequence of confocal images (Hutson *et al.*, 2003). The active contour or "snake" followed the bright fluorescent boundary between the amnioserosa cells and the adjacent lateral epidermis. In embryos expressing only green fluorescent *D*E-cadherin, the position of the leading edge of the lateral epidermis had to be estimated by its proximity to the boundary between the lateral epidermis and the amnioserosa. Here the amnioserosa cell boundaries display more prominent *D*E-cadherin fluorescence than the lateral epidermal cell boundaries. Amnioserosa cell boundaries that abutted the lateral epidermis were equally as bright as those from amnioserosa cells found more centrally in the dorsal opening. Nevertheless, the snake algorithm was able to produce reliable tracking of the true amnioserosa/lateral epidermis boundary, provided periodic human intervention was used to mask out brightly

fluorescent areas in the image that would otherwise detour the snake. This intervention was efficiently implemented with the paintbrush tool in the image processing program ImageJ (National Institutes of Health, Bethesda, MD) using an Intuos3 Wacom tablet and pen to paint a black mask over those brightly fluorescent areas that otherwise interfered with true tracking of the amnioserosa/leading-edge boundary.

Once the snakes algorithm produced snakes that accurately followed the amnioserosa/lateral epidermis boundary, the coordinates of those snake contours were read into a custom MATLAB program to calculate seven specific height measurements. As in previous publications, *H* represents the dorsal/ventral distance between the two opposing leading edges, as calculated along one particular column of pixels in the image (Hutson *et al.*, 2003). To ensure that this column of pixels measures along the dorsal/ventral axis of the embryo, images were rotated appropriately before snakes analysis.

Using the first captured image of the embryo, we took seven specific height measurements at points along the dorsal opening, including the symmetry point and three points to either side of it, each at a distance equal to 10% of the total anterior/posterior span of the snakes coordinates. We defined the symmetry point as the location along the dorsal opening with maximum height in that initial captured image. The maximum height in subsequent images may shift 1–2 pixels to the left or right of our chosen "symmetry point" location; however, we continue to call the same pixel location the symmetry point.

Curvature and leading-edge contraction measurements

The same snake points used for height calculations were also used to find curvature using a custom MATLAB script. Fiducial points were selected by hand in ImageJ at leading edge cell boundaries and followed over the course of the experiment to find leading edge contraction with a custom MATLAB script.

Amnioserosa cell boundary segmentation and analysis

Amnioserosa cells were automatically segmented by first classifying cell boundaries in each image. Blurring, filtering, and skeletonization produced a skeletonized, binary image of boundary traces from which individual amnioserosa cells were segmented. We used ImageJ for all image-processing procedures and a threshold-based method for segmentation and temporal tracking. We extracted quantitative parameters of each cell (area, centroid, position, different morphological descriptors); any incorrectly segmented or tracked cells upon visual inspection were discarded from further data analysis in MATLAB. Between 40 and 90% of the cells were accurately segmented and tracked using this approach; the effectiveness of segmentation was strongly dependent on image quality.

ACKNOWLEDGMENTS

We thank members of the Kiehart and Edwards lab for critical comments and discussions. This work was supported by National Institutes of Health GM33830 to D.P.K. and G.S.E., a National Science Foundation Graduate Research Fellowship to A.R.W., and Trinity College of Duke University Dean's Summer Research Fellowships to R.S.Z.

REFERENCES

Almeida L, Bagnerini P, Habbal A, Noselli S, Serman F (2011). A mathematical model for dorsal closure. J Theor Biol 268, 105–119.

Belacortu Y, Paricio N (2011). Drosophila as a model of wound healing and tissue regeneration in vertebrates. Dev Dyn 240, 2379–2404.

Blanchard GB, Murugesu S, Adams RJ, Martinez-Arias A, Gorfinkiel N (2010). Cytoskeletal dynamics and supracellular organisation of cell shape fluctuations during dorsal closure. Development 137, 2743–2752.

Copp AJ, Greene ND (2013). Neural tube defects—disorders of neurulation and related embryonic processes. Wiley Interdiscip Rev Dev Biol 2, 213–227.

David DJ, Tishkina A, Harris TJ (2010). The PAR complex regulates pulsed actomyosin contractions during amnioserosa apical constriction in Drosophila. Development 137, 1645–1655.

David DJ, Wang Q, Feng JJ, Harris TJ (2013). Bazooka inhibits aPKC to limit antagonism of actomyosin networks during amnioserosa apical constriction. Development 140, 4719–4729.

Fernandez BG, Arias AM, Jacinto A (2007). Dpp signalling orchestrates dorsal closure by regulating cell shape changes both in the amnioserosa and in the epidermis. Mech Dev 124, 884–897.

Fischer SC, Blanchard GB, Duque J, Adams RJ, Arias AM, Guest SD, Gorfinkiel N (2014). Contractile and mechanical properties of epithelia with perturbed actomyosin dynamics. PLoS One 9, e95695.

Franke JD, Montague RA, Kiehart DP (2005). Nonmuscle myosin II generates forces that transmit tension and drive contraction in multiple tissues during dorsal closure. Curr Biol 15, 2208–2221.

Gorfinkiel N, Blanchard GB, Adams RJ, Martinez Arias A (2009). Mechanical control of global cell behaviour during dorsal closure in *Drosophila*. Development 136, 1889–1898.

Gorfinkiel N, Schamberg S, Blanchard GB (2011). Integrative approaches to morphogenesis: lessons from dorsal closure. Genesis 49, 522–533.

Harden N (2002). Signaling pathways directing the movement and fusion of epithelial sheets: lessons from dorsal closure in *Drosophila*. Differentiation 70, 181–203.

Harris TJ, Sawyer JK, Peifer M (2009). How the cytoskeleton helps build the embryonic body plan: models of morphogenesis from Drosophila. Curr Top Dev Biol 89, 55–85.

Hunter GL, Crawford JM, Genkins JZ, Kiehart DP (2014). Ion channels contribute to the regulation of cell sheet forces during Drosophila dorsal closure. Development 141, 325–334.

Hutson MS, Tokutake Y, Chang MS, Bloor JW, Venakides S, Kiehart DP, Edwards GS (2003). Forces for morphogenesis investigated with laser microsurgery and quantitative modeling. Science 300, 145–149.

Jacinto A, Wood W, Balayo T, Turmaine M, Martinez-Arias A, Martin P (2000). Dynamic actin-based epithelial adhesion and cell matching during *Drosophila* dorsal closure. Curr Biol 10, 1420–1426.

Jankovics F, Brunner D (2006). Transiently reorganized microtubules are essential for zippering during dorsal closure in Drosophila melanogaster. Dev Cell 11, 375–385.

Jayasinghe AK, Crews SM, Mashburn DN, Hutson MS (2013). Apical oscillations in amnioserosa cells: basolateral coupling and mechanical autonomy. Biophys J 105, 255–265.

Keller R, Davidson LA, Shook DR (2003). How we are shaped: the biomechanics of gastrulation. Differentiation 71, 171–205.

Kiehart DP, Galbraith CG, Edwards KA, Rickoll WL, Montague RA (2000). Multiple forces contribute to cell sheet morphogenesis for dorsal closure in *Drosophila*. J Cell Biol 149, 471–490.

Kiehart DP, Tokutake Y, Chang M-S, Hutson MS, Wiemann J, Peralta XG, Toyama Y, Wells AR, Rodriguez A, Edwards GS (2006). Ultraviolet laser microbeam for dissection of *Drosophila* embryos. In: Cell Biology: A Laboratory Handbook, 3rd ed., Vol. 3, ed. JE Celis, San Diego, CA: Elsevier Academic Press, 87–103.

Layton AT, Toyama Y, Yang GQ, Edwards GS, Kiehart DP, Venakides S (2009). Drosophila morphogenesis: tissue force laws and the modeling of dorsal closure. HFSP J 3, 441–460.

Lecuit T, Lenne PF, Munro E (2011). Force generation, transmission and integration during cell and tissue morphogenesis. Annu Rev Cell Dev Biol 27, 157–184.

Ma X, Lynch HE, Scully PC, Hutson MS (2009). Probing embryonic tissue mechanics with laser hole drilling. Phys Biol 6, 036004.

Martin AC, Goldstein B (2014). Apical constriction: themes and variations on a cellular mechanism driving morphogenesis. Development 141, 1987–1998.

Mason FM, Tworoger M, Martin AC (2013). Apical domain polarization localizes actin-myosin activity to drive ratchet-like apical constriction. Nat Cell Biol 15, 926–936.

Miller CJ, Davidson LA (2013). The interplay between cell signalling and mechanics in developmental processes. Nat Rev Genet 14, 733–744.

Narasimha M, Brown NH (2004). Novel functions for integrins in epithelial morphogenesis. Curr Biol 14, 381–385.

Narasimha M, Uv A, Krejci A, Brown NH, Bray SJ (2008). Grainy head promotes expression of septate junction proteins and influences epithelial morphogenesis. J Cell Sci 121, 747–752.
Oda H, Tsukita S (1999). Dynamic features of adherens junctions during *Drosophila* embryonic epithelial morphogenesis revealed by a *D*a-catenin-GFP fusion protein. Dev Genes Evol 209, 218–225.
Oda H, Tsukita S (2001). Real-time imaging of cell-cell adherens junctions reveals that *Drosophila* mesoderm invagination begins with two phases of apical constriction of cells. J Cell Sci 114, 493–501.
Peralta XG, Toyama Y, Hutson MS, Montague R, Venakides S, Kiehart DP, Edwards GS (2007). Upregulation of forces and morphogenic asymmetries in dorsal closure during *Drosophila* development. Biophys J 92, 2583–2596.
Peralta XG, Toyama Y, Kiehart DP, Edwards GS (2008). Emergent properties during dorsal closure in *Drosophila* morphogenesis. Phys Biol 5, 015004.
Razzell W, Wood W, Martin P (2014). Recapitulation of morphogenetic cell shape changes enables wound re-epithelialisation. Development 141, 1814–1820.
Roberts DB (1998). *Drosophila*: A Practical Approach, Oxford, UK: IRL Press at Oxford University Press.
Rodriguez-Diaz A, Toyama Y, Abravanel DL, Wiemann JM, Wells AR, Tulu US, Edwards GS, Kiehart DP (2008). Actomyosin purse strings: renewable resources that make morphogenesis robust and resilient. HFSP J 2, 220–237.
Roh-Johnson M, Shemer G, Higgins CD, McClellan JH, Werts AD, Tulu US, Gao L, Betzig E, Kiehart DP, Goldstein B (2012). Triggering a cell shape change by exploiting preexisting actomyosin contractions. Science 335, 1232–1235.
Saravanan S, Meghana C, Narasimha M (2013). Local, cell-nonautonomous feedback regulation of myosin dynamics patterns transitions in cell behavior: a role for tension and geometry? Mol Biol Cell 24, 2350–2361.
Seelan RS, Mukhopadhyay P, Warner DR, Webb CL, Pisano M, Greene RM (2013). Epigenetic regulation of Sox4 during palate development. Epigenomics 5, 131–146.
Sokolow A, Toyama Y, Kiehart DP, Edwards GS (2012). Cell ingression and apical shape oscillations during dorsal closure in Drosophila. Biophys J 102, 969–979.
Solon J, Kaya-Copur A, Colombelli J, Brunner D (2009). Pulsed forces timed by a ratchet-like mechanism drive directed tissue movement during dorsal closure. Cell 137, 1331–1342.
Spahn P, Reuter R (2013). A vertex model of Drosophila ventral furrow formation. PLoS One 8, e75051.
Toyama Y, Peralta XG, Wells AR, Kiehart DP, Edwards GS (2008). Apoptotic force and tissue dynamics during *Drosophila* embryogenesis. Science 321, 1683–1686.
Wang Q, Feng JJ, Pismen LM (2012). A cell-level biomechanical model of Drosophila dorsal closure. Biophys J 103, 2265–2274.